Inorganic Chemistry

Article

pubs.acs.org/IC

Encapsulation of the 4-Mercaptobenzoate Ligand by Macrocyclic Metal Complexes: Conversion of a Metallocavitand to a Metalloligand

Jochen Lach,[†] Alexander Jeremies,[†] Daniel Breite,[‡] Bernd Abel,[‡] Benjamin Mahns,[§] Martin Knupfer,[§] Vitaly Matulis,[∥] Oleg A. Ivashkevich,[⊥] and Berthold Kersting*[,†]

[†]Institut für Anorganische Chemie, Universität Leipzig, D-04103 Leipzig, Germany

[‡]Chemische Abteilung, Leibniz Institut für Oberflächenmodifizierung eV, D-04318 Leipzig, Germany

[§]Leibniz Institute for Solid State and Materials Research, IFW Dresden, D-01171 Dresden, Germany

[∥]Research Institute for Physical Chemical Problems of Belarusian State University, Leningradskaya 14, 220030 Minsk, Belarus

[⊥]Belarusian State University, 4 Nezavisimisti Avenue, 220050 Minsk, Belarus

Supporting Information

ABSTRACT: Complexation of the ambidentate ligand 4-mercaptobenzoate (4-SH-$C_6H_4CO_2H$, H_2mba) by the macrocyclic complex $[Ni_2L(\mu\text{-Cl})]ClO_4$ (L^{2-} represents a 24-membered macrocyclic hexaazadithiophenolate ligand) has been examined. The monodeprotonated $Hmba^-$ ligand reacts with the Ni_2 complex in a selective manner by substitution of the bridging chlorido ligand to produce $\mu_{1,3}$-carboxylato-bridged complex $[Ni_2L(Hmba)]^+$ ($\mathbf{2}^+$), which can be isolated as an air-sensitive perchlorate ($\mathbf{2}ClO_4$) or tetraphenylborate ($\mathbf{2}BPh_4$) salt. The reactivity of the new mercaptobenzoate complex is reminiscent of that of a "free" thiophenolate ligand. In the presence of air, $\mathbf{2}ClO_4$ dimerizes via a disulfide bond to generate tetranuclear complex $[\{Ni_2L\}_2(O_2CC_6H_4S)_2]^{2+}$ ($\mathbf{3}^{2+}$). The auration of $\mathbf{2}ClO_4$ with $[AuCl(PPh_3)]$, on the other hand, leads to monoaurated complex $[Ni^{II}{}_2L(mba)Au^IPPh_3]^+$ ($\mathbf{4}^+$). The bridging thiolate functions of the N_6S_2 macrocycle are deeply buried and are unaffected/unreactive under these conditions. The complexes were fully characterized by electrospray ionization mass spectrometry, IR and UV/vis spectroscopy, density functional theory, cyclic voltammetry, and X-ray crystallography [for $\mathbf{3}(BPh_4)_2$ and $\mathbf{4}BPh_4$]. Temperature-dependent magnetization and susceptibility measurements reveal an $S = 2$ ground state that is attained by ferromagnetic coupling between the spins of the Ni^{II} ions in $\mathbf{2}ClO_4$ ($J = +22.3$ cm^{-1}) and $\mathbf{4}BPh_4$ ($J = +20.8$ cm^{-1}; $H = -2JS_1S_2$). Preliminary contact-angle and X-ray photoelectron spectroscopy measurements indicate that $\mathbf{2}ClO_4$ interacts with gold surfaces.

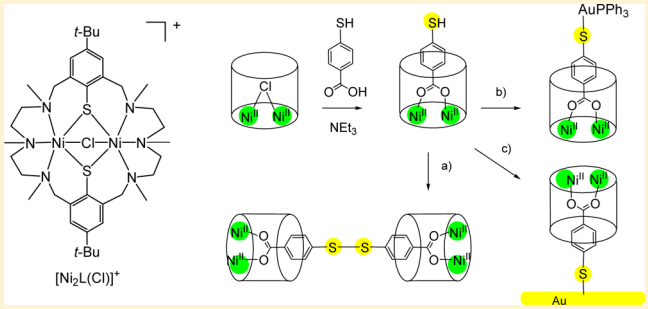

INTRODUCTION

The coordination chemistry of *o*-mercaptobenzoic acid (2-$HSC_6H_4CO_2H$), which is also known as thiosalicylic acid, has attracted much interest,[1] primarily because of its ability to form complexes with both hard and soft metal ions and the associated potential in several applications. Much research has focused on the preparation and characterization of thiosalicylato complexes of heavy metals such as gold(I), mercury(II), platinum(II),[2,3] and tin(II).[4,5] The gold compounds, for example, are of interest because of their supramolecular structures, which are governed by a combination of Au···Au interactions and hydrogen-bonding interactions as seen in $[Au(2\text{-}SC_6H_4CO_2H)(RNC)]$[6] and $[Au(2\text{-}SC_6H_4CO_2H)(PPh_3)]$.[7] The application of sodium ethylmercury thiosalicylate, $[EtHg(2\text{-}SC_6H_4CO_2Na)]$ (commonly known as thimerosal), in medicine and many other disciplines[8] is associated with its antimicrobial properties and has led to great interest in the structure, spectroscopic properties, and reactivity of mercury(II) thiosalicylate compounds.[9] A number of first-row transition-metal thiosalicylate complexes have also been structurally characterized previously. Jacobsen and Cohen used zinc tris(pyrazolylborate) complexes coligated by thiosalicylate ligands as models to augment and advance metalloproteinase inhibitor design.[10] Christou and co-workers used thiosalicylate to stabilize polynuclear vanadium(III) complexes such as $[PPh_4]_2[V_3OCl_4(2\text{-}HSC_6H_4CO_2)_5]$, whose anion contains a triangular $[V_3(\mu_3\text{-}O)]^{7+}$ core.[11] In view of these applications, it is somewhat surprising that the coordination chemistry of the para isomer of thiosalicylic acid, *p*-mercaptobenzoic acid (4-$HSC_6H_4CO_2H$, hereafter referred to as H_2mba), has been investigated far less frequently. Only a few discrete rhodium(I)[12] and gold(I) complexes[13,14] have been reported. Recently, the successful utilization of

Received: March 24, 2014
Published: October 9, 2014

dx.doi.org/10.1021/ic500683f | *Inorg. Chem.* 2014, 53, 10825−10834

H_2mba in the stabilization and surface chemical modification of gold nanoparticles[15] was demonstrated.

Following recent work in this group on the molecular recognition of carboxylato and dicarboxylato ligands by dinuclear $[Ni_2L]^{2+}$ complexes supported by the macrocyclic N_6S_2 donor ligand L (Figure 1),[16] we have turned our attention

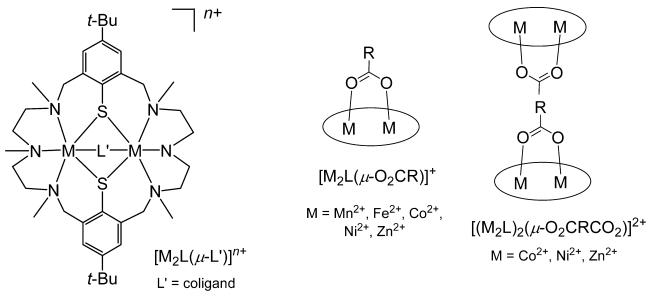

Figure 1. From left to right: Structure of dinuclear complexes $[M_2L(\mu\text{-}L')]^+$ of the macrocyclic ligand H_2L and representation of the structures of dinuclear and tetranuclear complexes with carboxylato and dicarboxylato ligands (the macrocycle L is shown as an ellipse for clarity).

to the encapsulation of the ambidentate H_2mba ligand. We show that the $[Ni_2L]^{2+}$ fragment binds the H_2mba ligand selectively via its carboxylate function and reports on the potential of the resulting $[Ni_2L(O_2CC_6H_4SH)]^+$ cation $\mathbf{2}^+$ to act as a monodentate thiolate ligand toward Au^I. The ability of H_2mba to act as a metalloligand toward different metal ions has precedence in the literature,[12] but the noncovalent protection of its carboxylate function by a dinuclear metallocavitand[17] represents a new strategy in the preparation of polynuclear H_2mba complexes.[18] The crystal structures, reactivity features, and magnetic and electrochemical properties of the new complexes are described.

RESULTS AND DISCUSSION

Synthesis and Characterization of Metal Complexes. The reaction of $[Ni_2L(\mu\text{-}Cl)]ClO_4$ ($\mathbf{1}ClO_4$) with H_2mba in CH_2Cl_2 in the presence of NEt_3 provides a green solution, from which a green, air-sensitive, microcrystalline product of composition $[Ni_2L(Hmba)]ClO_4$ ($\mathbf{2}ClO_4$) can be reproducibly obtained in yields as high as 88% (Scheme 1). The electrospray ionization mass spectrometry (ESI-MS) spectrum of $\mathbf{2}ClO_4$ with a base peak for the $[Ni_2L(Hmba)]^+$ dication (m/z 937.2 (95%); calcd m/z 937.2) and elemental analysis were clearly consistent with the formulation of a 1:1 complex.

Previous studies from these laboratories revealed that the $[Ni_2L]^{2+}$ dication has a high affinity for carboxylate ions,[16] but it can also bind thiophenolate.[19] To distinguish between the two binding modes in solution, we used UV/vis spectroscopy. The ν_1 ($^3A_{2g} \rightarrow {}^3T_{2g}$) and ν_2 ($^3A_{2g} \rightarrow {}^3T_{1g}$) transitions of these Ni_2 complexes are quite sensitive to the nature and type of the bridging coligand (ν_1 and ν_2 = 650 and 1121 nm for ($[Ni_2L(O_2CPh)]^+$),[20] 667 and 1141 nm for $[Ni_2L(SPh)]^+$). The electronic transitions recorded for $\mathbf{2}^+$ in MeCN solution (652 and 1125 nm) match better with those determined for $[Ni_2L(O_2CPh)]^+$. This suggests that $\mathbf{2}^+$ binds the $Hmba^-$ ligand via its carboxylate function. The latter coordination mode was further supported by IR spectroscopy. There are two bands at 1599 cm^{-1} [$\nu_{as}(RCO_2^-)$] and 1408 cm^{-1} [$\nu_{as}(RCO_2^-)$] attributable to a $\mu_{1,3}$-bridging carboxylate function. There are

Scheme 1. Synthesized Compounds and Their Labels

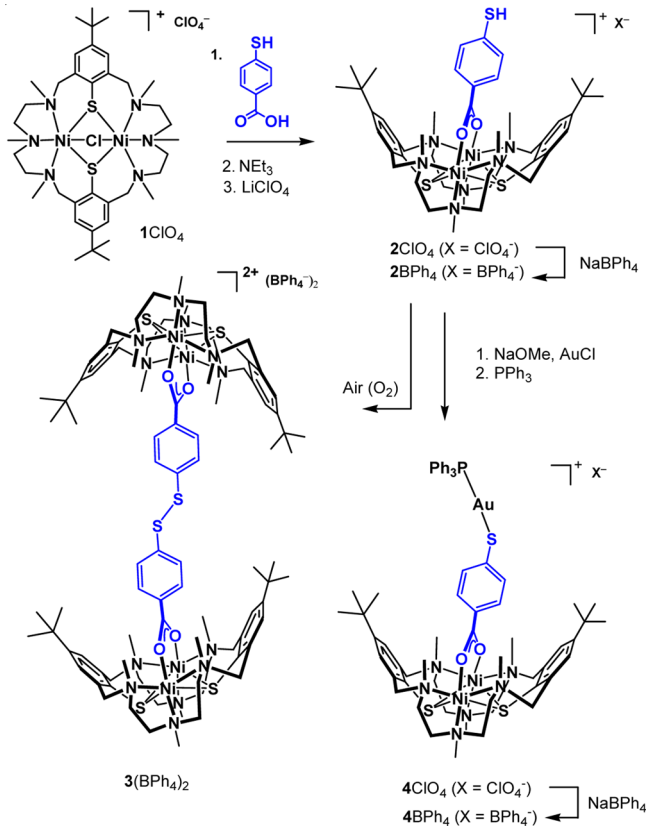

no peaks for a free RCO_2H function. However, a weak band at 2550 cm^{-1} ν(SH) typical for a RSH group is present.

To further confirm the presence of the carboxylato-bridged structure $\mathbf{2}^+$, we performed an exchange experiment (eq 1). When a solution of $[Ni_2L(SPh)]ClO_4$[19,21] in MeCN is treated with 1 equiv of NaO_2CPh, a color change from yellow to pale green takes place, and the resulting $[Ni_2L(O_2CPh)]ClO_4$ salt can be isolated in nearly quantitative yield. The energy (ΔE) of reaction (1) was calculated by density functional theory (DFT) methods. The reaction energy ΔE was found to be −10.6 kcal mol^{-1} in acetonitrile, indicating that $[Ni_2L(OCPh)]^+$ is substantially more stable than $[Ni_2L(SPh)]^+$. The higher affinity for the carboxylato group agrees with the fact that Ni^{2+} is a rather hard Lewis acid.[22] On the basis of these results, it can be concluded that the $[Ni_2L(Hmba)]^+$ complex binds the H_2mba ligand selectively via the carboxylate function.

$$[Ni_2L(SPh)]^+ + O_2CPh^- \rightarrow [Ni_2L(O_2CPh)]^+ + PhS^- \quad (1)$$

Efforts to obtain single crystals of $\mathbf{2}ClO_4$ or $[Ni_2L(Hmba)]$-BPh_4 ($\mathbf{2}BPh_4$) suitable for X-ray diffraction analysis proved unsuccessful. However, such crystals were obtained in the case of the oxidation product $[\{Ni_2L\}_2(O_2CC_6H_4S)_2](BPh_4)_2$ [$\mathbf{3}(BPh_4)_2$], which crystallizes from solutions of $\mathbf{2}BPh_4$ when exposed to air (Scheme 1). As can be seen (Figure 2), two $[Ni_2L(mba)]^+$ units are linked via a disulfide bond, with a distance of 13.510 Å between the center of the Ni···Ni axes of the dinuclear units. In $[(Ni_2L)_2(isophthalate)]^{2+}$, this distance is much smaller (9.561 Å).[23] Notice that the nickel-bound sulfur atoms are not affected by the oxidation.

We next explored the ability of complex $\mathbf{2}^+$ to act as a thiolato ligand toward gold.[24] Thiophenolate ligands are quite

dx.doi.org/10.1021/ic500683f | Inorg. Chem. 2014, 53, 10825−10834

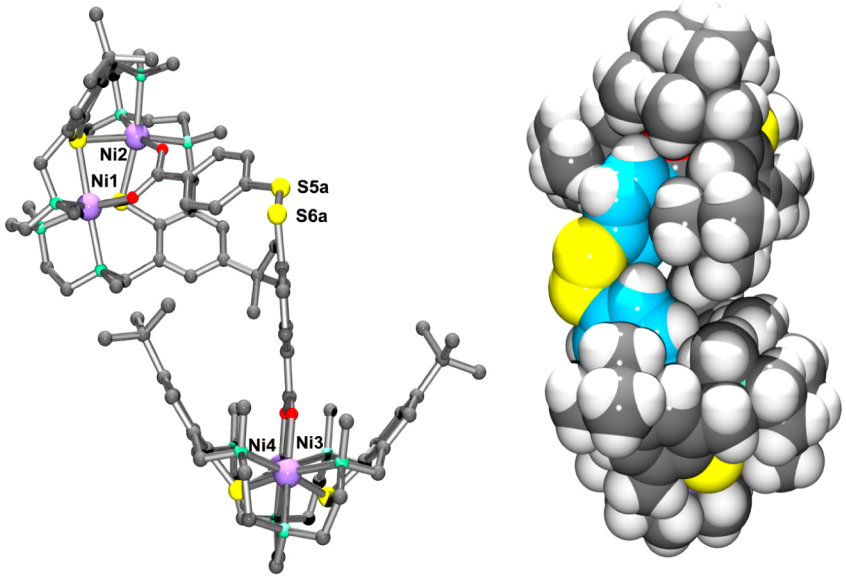

Figure 2. Ball-and-stick (left) and van der Waals (right) plots of the molecular structure of the $[(Ni_2L)_2(mba)_2]^{2+}$ dication in crystals of $\mathbf{3}(BPh_4)_2 \cdot n$EtOH$\cdot nCH_3$CN. Only one orientation of the disordered disulfide coligand is shown.

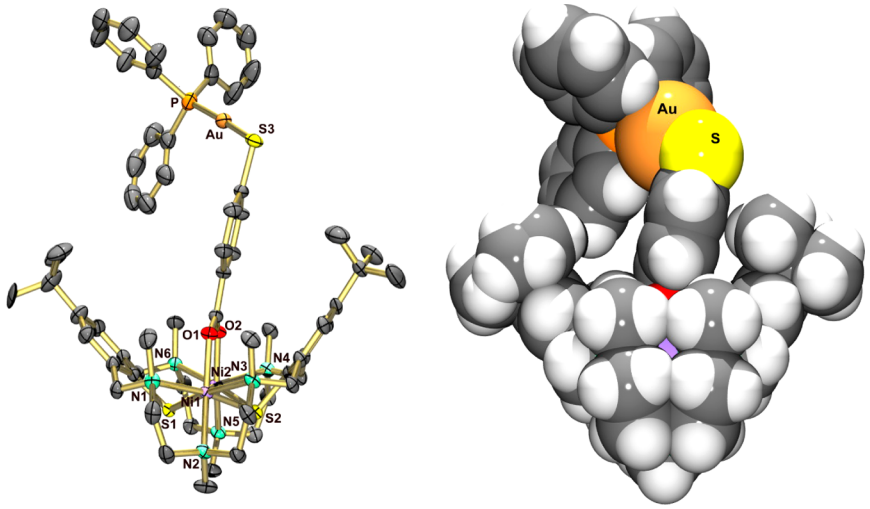

Figure 3. ORTEP (left) and van der Waals (right) plots of the molecular structure of the Ni_2Au complex $\mathbf{4}^+$ in crystals of $\mathbf{4}BPh_4 \cdot 2$MeCN$\cdot 2$EtOH. Thermal ellipsoids are at 50% probability. Selected bond lengths (Å) and angles (deg): Au−P 2.2620(13), Au−S3 2.3022(13); Ni1−O1 2.015(2), Ni1−S1 2.4445(11), Ni1−S2 2.4776(11), Ni1−N1 2.247(3), Ni1−N2 2.164(3), Ni1−N3 2.312(3), Ni2−S1 2.4488(10), Ni2−S2 2.4985(11), Ni2−O2 1.990(2), Ni2−N4 2.314(3), Ni2−N5 2.140(3), Ni2−N6 2.236(3), Ni1···Ni2 3.475(1); P−Au−S3 173.59(4), Ni1−S1−Ni2 90.48(4), Ni1−S2−Ni2 88.58(4).

aurophilic, and many gold(I) thiophenolate complexes have been described.[25] Indeed, when $\mathbf{2}ClO_4$ was allowed to react with an equimolar amount of $[AuCl(PPh_3)]$ in the presence of NaOMe at ambient temperature, trinuclear complex $[Ni_2L(mba)Au(PPh_3)]^+$ ($\mathbf{4}^+$) (ESI-MS: m/z 1397.4 (60% rel intens); calcd for $\mathbf{4}^+$ m/z 1397.4) forms, which can be isolated as perchlorate salt $[Ni_2L(mba)Au(PPh_3)]ClO_4$ in almost quantitative yields (>90%). The same compound forms also in the presence of a 3-fold excess of $[AuCl(PPh_3)]$, clearly evidencing that $\mathbf{2}ClO_4$ exhibits only one aurophilic thiophenolate function. In strong contrast to the thiol $\mathbf{2}ClO_4$, the aurated compound $[Ni_2L(O_2CC_6H_4S)AuPPh_3]ClO_4$ ($\mathbf{4}ClO_4$) is stable toward aerial oxidation for weeks in solution as well as in the solid state.

To ascertain the formulation of $\mathbf{4}^+$ as trinuclear complex $Ni^{II}_2Au^{I}$, it was characterized by X-ray crystallography as the tetraphenylborate salt $\mathbf{4}BPh_4 \cdot 2$MeCN$\cdot 2$EtOH, and its structure is shown in Figure 3. The coordination geometry about the gold atom is not perfectly linear (S−Au−P 173.59°), most likely because of steric interactions between the PPh_3 unit and the N_6S_2 macrocycle or crystal-packing effects.[26] In $[Au(SPh)(PPh_3)]$, the S−Au−P linkage is 179.0°.[27] The binding of the $Au^{I}PPh_3$ unit to the mercaptobenzoate does not significantly alter the structure of the $[Ni_2L(mba)]$ complex fragment. Thus, the aromatic ring of the mercaptobenzoate moiety is coplanar with the bridging carboxylato group, as observed in $\mathbf{3}(BPh_4)_2$. In essence, the mercaptobenzoate group in $\mathbf{2}ClO_4$ is the only potential binding site for gold atoms, and the binding does not alter the overall structure of the $[Ni_2L]^{2+}$ fragment.

Electrochemistry. In view of the air sensitivity of the thiolate complexes and the fact that the III+ oxidation state is attainable for nickel in a thiolate-rich coordination environ-

dx.doi.org/10.1021/ic500683f | Inorg. Chem. 2014, 53, 10825−10834

ment,[28−32] it was of interest to determine the redox properties of the $Ni^{II}Ni^{II}$ complexes $\mathbf{2}^+$ and $\mathbf{4}^+$ by cyclic voltammetry. Figure 4 shows the cyclic voltammogram (CV) of ca. 1×10^{-3} M acetonitrile solutions of $\mathbf{2}ClO_4$ and $\mathbf{4}ClO_4$ in acetonitrile. The CV of the acetato-bridged $Ni^{II}Ni^{II}$ complex $[Ni_2L(OAc)]ClO_4$ was reported previously[33] and is included for comparison.

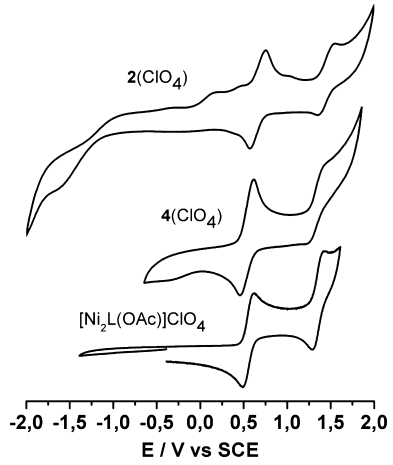

Figure 4. CVs of $\mathbf{2}ClO_4$ and $\mathbf{4}ClO_4$ in a CH_3CN solution at 298 K. The CV of $[Ni_2L(OAc)]ClO_4$ is shown for comparison. Experimental conditions: 0.1 M $[n\text{-}Bu_4N]PF_6$, ca. 1×10^{-3} M sample concentration; platinum disk working electrode; silver wire reference electrode; scan rate 100 mV s^{-1}; $[Co(Cp_2)]PF_6$ internal reference.

It is appropriate to discuss the CV of the $Ni^{II}{}_2Au^I$ complex $\mathbf{4}^+$ first. There are two consecutive waves, one at $E^1{}_{1/2} = +0.54$ V (vs SCE) with a peak-to-peak separation ΔE_p of 0.15 V and one at $E^2{}_{1/2} = +1.35$ V with $\Delta E_p = 0.15$ V. The CV is very similar to that of the acetato-bridged complex $[Ni^{II}{}_2L(OAc)]^+$, which shows two redox waves at $E^1{}_{1/2} = 0.56$ V and $E^2{}_{1/2} = 1.36$ V. The two redox processes in $[Ni^{II}{}_2L(OAc)]^+$ were previously assigned as metal-centered ($Ni^{II}Ni^{II} \rightarrow Ni^{III}Ni^{II}$) and ligand-based [$RS^-$(thiolate) → $RS^{\cdot}$(thiyl radical)] oxidation within the $[Ni^{II}{}_2L]^{2+}$ unit as represented in eqs 2 and 3. The similar behavior for $\mathbf{4}ClO_4$ implies that the first oxidation is metal-centered in nature and yields a mixed-valent $Ni^{III}Ni^{II}$ complex $\mathbf{4}^{2+}$, as indicated in eq 2. Indeed, controlled potential coulometry of a solution of the $Ni^{II}{}_2$ complex $\mathbf{4}^+$ in MeCN at 273 K at an applied potential of 1.0 V vs SCE consumed 0.97 (±0.03) e^-/complex, generating a deep-red solution, from which a deep-red microcrystalline solid of composition $[Ni^{III}Ni^{II}L(mba)Au(PPh_3)](ClO_4)_2$ [$\mathbf{4}(ClO_4)_2$] can be isolated.[34] The CV of this material is identical with that of the parent complex ($\mathbf{4}ClO_4$), and rereduction of $\mathbf{4}(ClO_4)_2$ at a potential of 0 V reforms the monocation $\mathbf{4}^+$, indicating that complex $\mathbf{4}^+$ retains its integrity upon oxidation. The fully oxidized $Ni^{III}Ni^{II}$ form $\mathbf{4}^{3+}$ is only stable on the time scale of the CV experiment. Attempts to access the trication $\mathbf{4}^{3+}$ by controlled potential coulometry were unsuccessful and led to decomposition of the Ni_2Au complex to unknown products.

$$\underset{\mathbf{4}^+}{[Ni^{II}Ni^{II}L(mba)Au(PPh_3)]^+} \underset{+e^-}{\overset{-e^-}{\rightleftharpoons}} \underset{\mathbf{4}^{2+}}{[Ni^{III}Ni^{II}L(mba)Au(PPh_3)]^{2+}} \quad (2)$$

$$\underset{\mathbf{4}^{2+}}{[Ni^{III}Ni^{II}L(mba)Au(PPh_3)]^{2+}} \underset{+e^-}{\overset{-e^-}{\rightleftharpoons}} \underset{\mathbf{4}^{3+}}{[Ni^{III}Ni^{II}L^{\bullet}(mba)Au(PPh_3)]^{3+}} \quad (3)$$

The redox chemistry of two-coordinate Au^I complexes is known.[35] Neutral Au^I complexes generally undergo an irreversible reduction to Au^0 at very cathodic potentials below −2.0 V.[36] The form and position of the reduction peaks also depend on gold coverage of the electrode. In our chosen potential window ranging from −2 to +2.5 V vs SCE, there are no further redox waves, which can be attributed to reduction of the mba-$Au^I(PPh_3)$ group in good agreement with the reported trend.[36] It can be concluded that this unit is redox-inactive in this potential range.

Overall, the $\mathbf{4}^+$ complex undergoes a reversible one-electron oxidation reaction, which is accompanied by a change of the spin ground state from $S = 2$ for the $Ni^{II}Ni^{II}$ form $\mathbf{4}^+$ to $S = {}^3/_2$ for the mixed-valent $Ni^{II}Ni^{III}$ form $\mathbf{4}^{2+}$ (see below).[37] The CV data further show that formation of the Au^I−S bond is an effective protecting group for the air-sensitive thiolate group.

The CV of $\mathbf{2}ClO_4$ is similar but not identical with that of $\mathbf{4}ClO_4$. The two peaks at 0.66 and 1.45 V vs SCE can be assigned in the same manner as that for $\mathbf{4}^+$. The CV shows an additional, less-well-defined feature in the cathodic potential regime with peak potentials of $E_p^{red} \sim -1.6$ V and $E_p^{ox} \sim -1.0$ V. These features are tentatively assigned to reduction and oxidation of the 4-mercaptobenzoate ligand. However, determination of the $RS^-/RSSR$ couple may be hampered because of chemisorption of thiolate ligands to the electrode

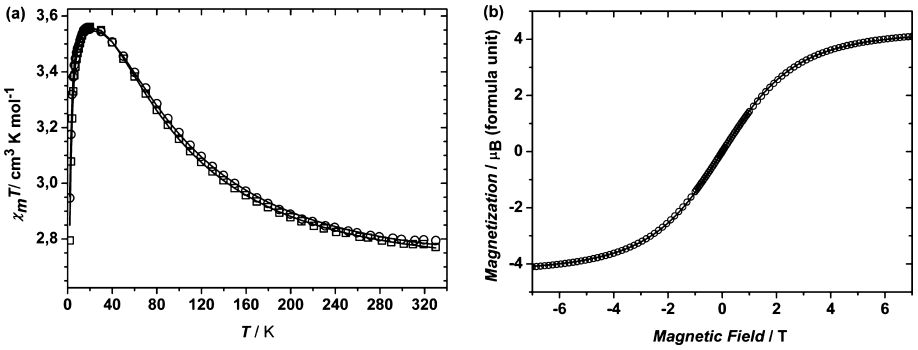

Figure 5. Left: Temperature dependence of the magnetic susceptibility (per dinuclear complex) for $\mathbf{2}ClO_4$ (open circles) and $\mathbf{4}ClO_4$ (open squares). The full lines represent the best theoretical fit to eq 5. Right: Field dependence of the magnetization of $\mathbf{2}ClO_4$ (open circles). The full line represents the best theoretical fit to eq 4 with $S = 2$, $T = 4$ K, and $g = 2.14$. Experimental and calculated values are provided in the Supporting Information.

dx.doi.org/10.1021/ic500683f | Inorg. Chem. 2014, 53, 10825−10834

material.[35] Therefore, these values should be taken as indicative rather than definitive.

Electronic Structures of Complexes $2ClO_4$ and $4ClO_4$. Complexes $2ClO_4$ and $4ClO_4$ were further characterized by temperature-dependent magnetic susceptibility measurements to determine their electronic structures. The magnetic susceptibility measurements were carried out on powdered solid samples in the temperature range between 2 and 330 K at an applied external magnetic field of 0.5 T using a MPMS 7XL SQUID magnetometer (Quantum Design). Figure 5 displays the temperature dependence of the molar magnetic susceptibility (per dinuclear complex) in the form of a $\chi_M T$ versus T plot. For $2ClO_4$, the value of $\chi_M T$ increases from 2.79 cm^3 K mol^{-1} (4.73 μ_B) at 330 K to a maximum value of 3.55 cm^3 K mol^{-1} (5.33 μ_B) at 20 K and then decreases to 2.95 cm^3 K mol^{-1} (4.86 μ_B) at 2 K. Virtually the same behavior can be noted for complex $4ClO_4$. Here the value of $\chi_M T$ increases from 2.77 cm^3 K mol^{-1} (4.71 μ_B) at 330 K to a maximum value of 3.56 cm^3 K mol^{-1} (5.34 μ_B) at 20 K and then decreases to 2.79 cm^3 K mol^{-1} (4.73 μ_B) at 2 K. The decrease in $\chi_M T$ below 20 K can be attributed to zero-field splitting of Ni^{II}. The magnetic susceptibility behavior is in both cases characteristic for an intramolecular ferromagnetic exchange interaction between two Ni^{II} ions, leading to an $S = 2$ ground state. The data also show that auration does not significantly influence the electronic structure of the $[Ni_2L(mba)]^{2+}$ complex fragment, a fact that is not surprising given the diamagnetic d^{10} configuration of the $RS-Au^{I}-PPh_3$ unit.

In order to confirm the $S = 2$ ground state, a field-dependent magnetization measurement of $2ClO_4$ was carried out at 4 K between −7 and +7 T using a MPMS 7XL SQUID magnetometer (Quantum Design). Figure 5 shows the field dependence of the molar magnetization in the form of a M versus H plot together with the theoretical fit derived from the Brillouin function (eq 4) for 2^+. As can be seen, a good fit was possible over the full temperature range, clearly indicative of an $S = 2$ ground state.

$$M(H)_{\text{Brillouin}} = N_A g \mu_B \left[\frac{2S+1}{2S} \coth\left(\frac{g\mu_B H}{kT} \frac{2S+1}{2S} \right) - \frac{1}{2S} \coth\left(\frac{g\mu_B H}{kT} \frac{1}{2S} \right) \right] \quad (4)$$

In order to quantify the magnitude of the magnetic exchange interaction, the experimental $\chi_M T$ versus T data were analyzed using the spin Hamiltonian in eq 5 including the isotropic Heisenberg–Dirac–van Vleck (HDvV) exchange, the single-ion zero-field splitting, and the single-ion Zeeman interactions using a full-matrix diagonalization approach.[38−,40]

$$H = -2J\hat{S}_1\hat{S}_2 + \sum_{i=1}^{2} \left\{ D_i \left[\hat{S}_{zi}^{\,2} - \frac{1}{3}\hat{S}_i(\hat{S}_i + 1) \right] + g_i \mu_B S_{i\tau} B_\tau \right\} \quad (\tau = x,\ y,\ z) \quad (5)$$

The experimental data of $2ClO_4$ and $4ClO_4$ were fitted to eq 5 over the full temperature range, assuming identical isotropic g values for the two Ni^{II} ions. The parameters of 2^+ and 4^+ leading to the best fits are listed in Table 1. The parameters determined for 2^+ were $J = +22.3$ cm^{-1}, $g = 2.18$, $D = 5.2$ cm^{-1}, and TIP = 3.6×10^{-4} cm^3 mol^{-1} (TIP = temperature-independent paramagnetism). In the case of 4^+, the best fit to the experimental data yielded $J = +20.8$ cm^{-1}, $g = 2.18$, $D = 6.7$ cm^{-1}, and TIP = 3.3×10^{-4} cm^3 mol^{-1}. Even though inclusion of the zero-field-splitting parameter generally improves the quality of the fit, one must be aware that these values should be taken as indicative rather than definite. It should be mentioned that all other carboxylato-bridged Ni^{II}-complex-supported L^{2-} show a weak ferromagnetic exchange coupling. The J values for $[Ni_2L(OAc)]BPh_4$ and $[Ni_2L(O_2CPh)]BPh_4$ at 21.7 and 18.4 cm^{-1}, respectively, are very similar to those in 2^+ and 4^+.[41]

Table 1. Magnetic Properties of Complexes $2ClO_4$ and $4ClO_4$ and Other Carboxylato-Bridged Ni_2 Complexes Supported by the N_6S_2 Macrocycle[a]

compound	g	J, cm^{-1}	D, cm^{-1}	TIP, cm^3 mol^{-1}
$2ClO_4$	2.18	22.29	5.23	3.59×10^{-4}
$4ClO_4$	2.18	20.83	6.73	3.33×10^{-4}
$[Ni_2L(OAc)]ClO_4$[41]	2.14	21.7	8.6	
$[Ni_2L(O_2CPh)]ClO_4$[41]	2.19	18.4	4.4	

[a]Parameters resulting from least-squares fit to the $\chi_M T$ data under the spin Hamiltonian in eq 5: J = coupling constant ($H = -2JS_1S_2$), $g = g$ value, D = zero-field-splitting parameter, and TIP = temperature-independent paramagnetism.

Chemisorption of $2ClO_4$ on Gold. There is currently great interest in the stabilization of gold nanoparticles by the 4-mercatobenzoate ligand. The Kornberg group, for example, obtained particles sufficiently uniform in size for the growth of large single crystals, suitable for X-ray structure determination, resulting in the first unambiguous structural characterization of a thiol-protected gold nanoparticle.[15] On these grounds, we decided to study the chemisorption of $2ClO_4$ on gold. The deposition of $2ClO_4$ was performed in analogy to the preparation of self-assembled thiol monolayers on gold as described in the literature.[42] A clean gold-coated silicon wafer was immersed in a 1×10^{-3} M solution of $2ClO_4$ in EtOH for 24 h followed by washing with EtOH and drying. The wettability of the surface was expected to change with chemisorption of the thiolate complexes, and so immobilization of the complexes was probed using static water-contact-angle measurements. Table 2 lists the results.

Table 2. Water (static)-Contact-Angle Measurement Obtained for Gold Films Modified with Various Dinickel(II) Complexes[a]

entry	compound	contact angle (deg)
1	bare gold (EtOH)	75.8 (1.5)
2	H_2mba	55.6 (1.7)
3	$2ClO_4$	71.4 (2.1)
4	$2BPh_4$	75.9 (2.1)
5	$2ClO_4$ (after metathesis with $NaBPh_4$)	76.0 (2.0)
6	$[Ni_2L(OAc)]ClO_4$	75.9 (2.0)

[a]The values represent the average of 10 measurements using 4 μL drops of deionized water. Standard deviations are given in parentheses. The "bare" gold surfaces were identically treated to the modified surfaces except with omission of any adsorbate in the solvent.

The contact-angle measurements showed small but significant variations, indicating that the complexes bind indeed to the gold surface. For the unmodified gold-containing adventitious, nonpolar material, a contact angle of 75.8° is obtained, which agrees with the value reported in the literature.[43] The contact angle of the free $Hmba^-$ ligand is lower than that of bare gold, in good agreement with the

dx.doi.org/10.1021/ic500683f | Inorg. Chem. 2014, 53, 10825−10834

presence of polar surface carboxylate functions.[44] The value of 55.6° is relatively high for a carboxylate-terminated monolayer, suggesting that the CO_2H groups are involved in intermolecular hydrogen-bonding interactions. Such an effect is known to increase the hydrophobicity of rather polar molecules and has been observed by others.[45,46] Upon chemisorption of the $\mathbf{2}ClO_4$ complex, the contact angle reduces slightly relative to the unmodified gold, indicating a surface transition to a more hydrophilic state. This is not surprising given the presence of a charged surface complex. The contact angle for chemisorbed $\mathbf{2}ClO_4$ on gold is comparable with those of alkanethiol monolayers terminated with ester, alkoxy, or thioester groups.[47] The angle seems to be quite high for an ionic compound, but we emphasize here that the charges are well shielded by the apolar groups of the macrocyclic ligands. A thin film of the more lipophilic tetraphenylborate salt $\mathbf{2}BPh_4$ on gold increases the contact angle by 4.5° (Table 2, entry 4), which would be expected because the BPh_4^- group is even more hydrophobic than the ClO_4^- ion. The contact-angle measurements also revealed that complexes such as $[Ni_2L(OAc)]ClO_4$, which lack end groups for surface fixation, are not chemisorbed on the gold surfaces (entry 6). It is worth mentioning that the ClO_4^- anions of immobilized $\mathbf{2}ClO_4$ can be exchanged by BPh_4^- ions in a surface metathesis reaction. Thus, chemisorbed $\mathbf{2}ClO_4$ on gold upon treatment with $NaBPh_4$ undergoes an anion-exchange reaction to produce $\mathbf{2}BPh_4$, as indicated by the change of the contact angle (entry 5). The chemisorbed cationic complexes $\mathbf{2}^+$ remain attached to the surfaces. Such anion-exchange reactions have been observed by others, e.g., for polycations attached to solid surfaces.[48]

XPS Studies. The attachment of $\mathbf{2}ClO_4$ to the gold surface was further analyzed by X-ray photoelectron spectroscopy (XPS). XPS spectra were recorded for bulk $\mathbf{2}ClO_4$ and for $\mathbf{2}ClO_4$ chemisorbed on gold. However, the long exposure time led to significant X-ray-induced damages; particularly affected are the ClO_4^- groups and the bridging thiolate sulfur atoms of the N_6S_2 macrocycle, as further detailed below. Table 3 lists selected peak positions and their assignments.

Table 3. XPS Binding Energies (eV) for $\mathbf{2}ClO_4$ and Monolayers of $\mathbf{2}ClO_4$ on Gold[a]

element	$\mathbf{2}ClO_4$	$\mathbf{2}ClO_4$ on Au(111)	assignment
$S(2p_{3/2})$	169.2	168.7	RSO_3^-
	163.0	163.6	nickel-bound sulfur atoms
	164.3		free thiol
		161.9	gold-bound 4-mercaptobenzoate
$S(2p_{1/2})$	170.2	169.7	RSO_3^-
	164.1	164.6	nickel-bound sulfur atoms
	165.3		free thiol
		162.8	gold-bound 4-mercaptobenzoate
$Ni(2p_{3/2})$	856.3	855.0	Ni^{2+}
	863.0	862.5	"shake up satellite"
C(1s)	286.1	285.2	aliphatic and aromatic carbon atoms
	287.5	286.6	sulfur-bound carbon atoms
	289.5	288.6	RCO_2^-
$Cl(2p_{3/2})$	208.8	209.0	ClO_4^-
$Cl(2p_{1/2})$	210.4	210.6	
$Cl(2p_{3/2})$	199.5	199.0	Cl^-
$Cl(2p_{1/2})$	201.1	200.6	

[a]The binding energies are referenced to $Au(4f_{7/2})$ (84.0 eV)

The XPS spectra for $\mathbf{2}ClO_4$ and for a monolayer of $\mathbf{2}ClO_4$ on gold in the S(2p) region clearly reveal the covalent attachment of the $[Ni_2L(mba)]^+$ complexes to the gold surface via Au–S single bonds (Figure 6). The XPS spectrum of bulk $\mathbf{2}ClO_4$

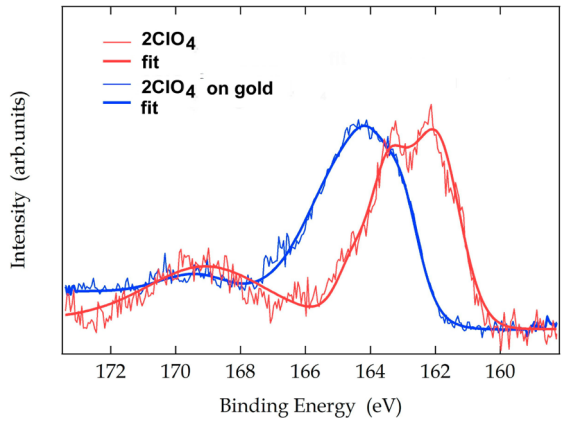

Figure 6. XPS $S(2p_{3/2})$ and $S(2p_{1/2})$ peaks for bulk $\mathbf{2}ClO_4$ and for $\mathbf{2}ClO_4$ chemisorbed on gold.

shows two sulfur photopeaks at binding energies of 164.3 and 163.0 eV, in agreement with the presence of the two kinds (one free thiol group and two nickel-bound thiolate sulfur atoms) of sulfur atoms. Upon binding to the gold surface, one of these peaks is significantly shifted from 164.3 to 161.9 eV, whereas the other shifts only slightly from 164.3 to 163.6 eV. The latter peak is therefore assigned to the bridging thiophenolate sulfur atoms because their bonding situation does not change upon surface functionalization.[49] The other features are attributed to the free thiol function (164.3 eV) in $\mathbf{2}ClO_4$ and the gold-bound thiolate atoms (161.9 eV) in $\mathbf{2}ClO_4$ chemisorbed on gold. These binding energies are typical for free thiol[50] and gold-bound thiolate sulfur atoms.[51] The absence of free signals for thiols also rules out the presence of overlayers.

The features at higher energies (169.2 and 168.7 eV) are assumed to be due to a sulfonate group (RSO_3^-). The oxygen atoms most likely arise from X-ray-induced decomposition of the ClO_4^- ions. Decomposition of ClO_4^- by X-rays has been reported previously.[52] It indicates that some of the RS^- groups in $\mathbf{2}ClO_4$ groups are oxidized to RSO_3^- groups, as seen in bulk $\mathbf{2}ClO_4$. It is worth mentioning that oxygenation reactions of $[Ni_2L(carboxylato)]^+$ complexes with H_2O_2 and *m*-chloroperoxybenzoic acid[41] convert the bridging thiolate to sulfonate groups without gross structural changes of the complexes, and it is assumed that similar conversions take place in the chemisorbed complexes.

Figure 7 shows the photoelectron peaks in the $Ni(2p_{3/2})$ region for bulk $\mathbf{2}ClO_4$ and for $\mathbf{2}ClO_4$ chemisorbed on gold. The binding energies differ slightly; however, the shape of the $Ni(2p_{3/2})$ signals with well-known shakeup satellites at 863 and 862.5 eV is characteristic for divalent, six-coordinate nickel complexes. These data imply that complex $\mathbf{2}^+$ undergoes no redox changes upon surface fixation.[53−56] The Cl(2p) regions show the presence of ClO_4^- ions (209 eV), and the additional spectral features (199.5 and 201.1 eV) correspond to chloride ions. This is the result of photoinduced decomposition of the ClO_4^- ion into Cl^- and has been reported previously.[52]

Photoelectron peaks of carbon and oxygen are also observed (Supporting Information). The C(1s) signal can be deconvoluted into three signals. The strong C(1s) signal at 285.2 eV

dx.doi.org/10.1021/ic500683f | Inorg. Chem. 2014, 53, 10825−10834

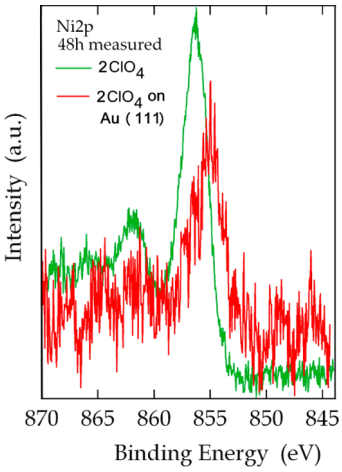

Figure 7. XPS Ni($2p_{3/2}$) peaks for bulk **2**ClO_4 and **2**ClO_4 chemisorbed on gold.

can be attributed to the aliphatic and aromatic (CH) carbon atoms of the 4-mercaptobenzoate and N_6S_2 aminothiophenolate ligands. The peak at 286.6 eV is attributed to the three electron-deficient carbon atoms bonded to electronegative sulfur atoms.[57] There is also a weak peak at 288.6 eV, which can be attributed to the carboxylate function.[51] The Cl(2p) region shows that the ClO_4^- ions (208 eV) are incorporated into the monolayers. Altogether, the XPS spectrum provides strong evidence for a covalent Au−S linkage between $\mathbf{2}^+$ and the gold surface in a monolayer.

SUMMARY

The main findings of the present work can be summarized as follows: (i) The dinuclear Ni^{II} complex $[Ni_2L(Hmba)]^+$ ($\mathbf{2}^+$), where L is a macrocyclic hexaminedithiophenolate ligand and $Hmba^-$ is 4-mercaptobenzoate, is readily prepared and can be isolated as an air-sensitive perchlorate **2**ClO_4 or tetraphenylborate $[Ni_2L(Hmba)]BPh_4$ (**2**BPh_4) salt. (ii) The X-ray structure determination showed that the ambidentate 4-mercaptobenzoate coligand binds specifically, via its carboxylate function, to the $[Ni_2L]^{2+}$ fragment such that the soft thiol function is positioned in the periphery of the complex. (iii) The mode of auration of **2**ClO_4 with $[AuCl(PPh_3)]$ demonstrates that **2**ClO_4 exhibits only one gold binding site. Only the thiolate function of the $Hmba^-$ ligand is aurated. The two thiolate sulfur atoms in **2**ClO_4 exhibit no aurophilicity. (iv) The $[Ni^{II}_2L(Hmba)]^+$ and $[Ni^{II}_2L(mba)Au(PPh_3)]^+$ complexes exhibit an $S = 2$ ground state that is attained by ferromagnetic coupling of the two Ni^{II} ($S_i = 1$) ions. (v) The $[Ni_2L(Hmba)]^+$ complex is redox-active and is also accessible in a mixed-valent $Ni^{II}Ni^{III}$ form of a different $S = {}^3/_2$ ground spin state. (vi) Complexes of **2**ClO_4 can be chemisorbed on gold surfaces via the formation of Au−S surface bonds, as was clearly established by contact-angle and XPS measurements.

EXPERIMENTAL SECTION

Materials and Methods. All reagents were purchased from commercial sources unless otherwise specified. Compound **1**ClO_4 was prepared as described in the literature. Ethanol (EtOH) was deoxygenated with nitrogen prior to use. Acetonitrile was distilled from calcium hydride. The syntheses of the metal complexes were carried out under a protective atmosphere of nitrogen. Melting points were determined in open glass capillaries and are uncorrected. The IR spectra were recorded as KBr disks using a Bruker Tensor 27 FT-IR spectrophotometer. UV/vis spectra were recorded on a Jasco V-670 UV/vis/near-IR spectrophotometer. Elemental analyses were carried out on a Vario EL elemental analyzer. ESI-MS spectra were recorded on a Bruker Daltronics ESQUIRE3000 PLUS spectrometer. Elemental analyses were carried out on a Vario EL elemental analyzer. Cyclic voltammetry measurements were carried out at 25 °C with an EG&G Princeton Applied Research model 263 A potentiostat/galvanostat. The cell contained a platinum working electrode, a platinum wire auxiliary electrode, and a silver wire reference electrode. The concentrations of the solutions were 1.0×10^{-1} M in supporting electrolyte $N^nBu_4PF_6$ and ca. 1.0×10^{-3} M in the sample. Cobaltocenium hexafluorophosphate (Cp_2CoPF_6) was used as an internal standard. All potentials are given versus SCE but are standardized against the ferrocenium/ferrocene couple.[58] Temperature-dependent magnetic susceptibility measurements on powdered solid samples were carried out using a MPMS 7XL SQUID magnetometer (Quantum Design) over the temperature range 2−330 K at an applied magnetic field of 0.5 T. The observed susceptibility data were corrected for underlying diamagnetism. ***Caution!*** *Perchlorate salts of transition-metal complexes are hazardous and may explode. Only small quantities should be prepared, and great care should be taken.*

*$[Ni_2L(O_2CC_6H_4SH)]ClO_4$ (**2**ClO_4).* To a nitrogen-purged solution of 4-mercaptobenzoic acid (22 mg, 0.14 mmol) in CH_2Cl_2 was added triethylamine (0.15 mL, 0.14 mmol). Solid **1**ClO_4 (100 mg, 0.108 mmol) in MeOH (25 mL) was added. The resulting green solution was stirred for 48 h and filtered. A nitrogen-purged solution of $LiClO_4 \cdot 3H_2O$ (87.1 mg. 0.54 mmol) in EtOH (30 mL) was added, and then the solvent volume was reduced in vacuo to about 10 mL. The resulting green precipitate was filtered off, washed with EtOH, and dried in vacuo to give 99 mg (88%) of **1**ClO_4 as an air-sensitive, green, microcrystalline powder. Mp: 320−324 °C (dec). IR (KBr pellet, cm^{-1}): ν 3445 (s), 2961 (s), 2867 (w), 2807 (w), 2741 (w), 2550 (w, ν(SH)), 1717 (w), 1594 (s, $\nu_{as}(RCO_2^-)$), 1554 (s), 1486 (w), 1462 (m), 1422 (w), 1404 (s, $\nu_{symm}(RCO_2^-)$), 1363 (w), 1350 (w), 1309 (w), 1292 (w), 1264 (m), 1233 (m), 1201 (w), 1177 (w), 1171 (w), 1153 (w), 1096 (s), 1059 (w), 1039 (w), 1014 (w), 1001 (w), 982 (w), 931 (w), 913 (m), 881 (m), 843 (w), 825 (s), 817 (w), 807 (w), 766 (m), 753 (w), 722 (w), 689 (w), 668 (w), 623 (m), 600 (w), 564 (w), 540 (w), 493 (w), 473 (w), 436 (w), 416 (w). UV/vis [CH_2Cl_2; λ_{max}, nm (ε, M^{-1} cm^{-1})]: 265 (30603), 305 (12398), 329 (9868), 374sh (1835), 456sh (136), 652 (32, $^3A_{2g} \rightarrow {}^3T_{1g}$), 912sh (15, $^3A_{2g} \rightarrow {}^1E_g(D)$), 1125 (60, $^3A_{2g} \rightarrow {}^3T_{2g}$). ESI-MS ($CH_3CN$): m/z 937.2 (95%); calcd for $[Ni_2L(\mu\text{-}O_2CC_6H_4SH)]^+$ m/z 937.2. Elem anal. Calcd for $C_{45}H_{69}ClN_6Ni_2O_6S_3 \cdot 2H_2O$ (1039.01 + 36.03): C, 50.27; H, 6.84; N, 7.82. Found: C, 50.31; H, 6.98; N, 7.60.

*$[Ni_2L(O_2CC_6H_4SH)]BPh_4$ (**2**BPh_4).* To a solution of the perchlorate salt **2**ClO_4 (100 mg, 0.10 mmol) in dichloromethane (40 mL) was added with constant stirring a solution of $NaBPh_4$ (165 mg, 0.48 mmol) in EtOH (30 mL). The volume of the reaction mixture was reduced to about 5 mL. The resulting green precipitate was isolated by filtration, washed twice with EtOH and ether, and dried in vacuo. Yield: 108 mg (0.09 mmol, 86%). IR (KBr pellet, cm^{-1}): ν 3442 (s), 3135 (w), 3054 (w), 3037 (w), 2998 (w), 2963 (s), 2866 (m), 2807 (w), 2740 (w), 2553 (w, ν(SH)), 1716 (w), 1594 (s, $\nu_{as}(RCO_2^-)$), 1553 (m), 1480 (w), 1461 (m), 1422 (w), 1404 (s, $\nu_{symm}(RCO_2^-)$), 1363 (w), 1350 (w), 1308 (w), 1291 (w), 1266 (m), 1233 (m), 1200 (w), 1178 (w), 1152 (w), 1112 (w), 1077 (s), 1057 (w), 1041 (w), 1014 (w), 982 (w), 930 (w), 912 (m), 881 (m), 844 (w), 824 (s), 817 (w), 807 (w), 766 (w), 733 (m), 705 (s), 668 (w), 631 (m), 613 (m), 605 (w), 563 (w), 541 (w), 493 (w), 472 (w), 435 (w), 417 (w). UV/vis [CH_2Cl_2; λ_{max}, nm (ε, M^{-1} cm^{-1})]: 266 (44867), 306 (14151), 330 (11141), 374sh (2047), 456sh (170), 651 (43, $^3A_{2g} \rightarrow {}^3T_{1g}$), 913sh (18, $^3A_{2g} \rightarrow {}^1E_g(D)$), 1124 (68, $^3A_{2g} \rightarrow {}^3T_{2g}$). ESI-MS ($CH_3CN$): m/z 937.2 (95%); calcd for $[Ni_2L(\mu\text{-}O_2CC_6H_4SH)]^+$ m/z 937.2. Elem anal. Calcd for $C_{69}H_{89}BN_6Ni_2O_2S_3 \cdot H_2O$ (1258.88 + 18.01): C, 64.90; H, 7.18; N, 6.58. Found: C, 64.63; H, 7.10; N, 6.39.

*$[\{Ni_2L\}_2(O_2CC_6H_4S)_2](BPh_4)_2$ [**3**$(BPh_4)_2$].* A solution of the tetraphenylborate salt **2**BPh_4 (126 mg, 0.10 mmol) in dichloromethane/EtOH (40 mL) was exposed to air for 12 h. The volume of the reaction

dx.doi.org/10.1021/ic500683f | Inorg. Chem. 2014, 53, 10825−10834

Table 4. Total Energies for $[Ni_2L(SPh)]^+$, O_2CPh^-, $[Ni_2L(O_2CPh)]^+$, and PhS^- and Reaction Energy According to PBE0/TZV(P) (or PBE0/TZVP) Calculations

total energy (E), au				
$[Ni_2L(SPh)]^+$	O_2CPh^-	$[Ni_2L(O_2CPh)]^+$	PhS^-	reaction energy (ΔE), kcal
−6299.52360	−420.28045	−6088.40245	−631.43096	−18.4[a]
−6299.59261	−420.38397	−6088.46850	−631.52491	−10.6[b]
−6299.67500	−420.39203	−6088.55104	−631.53307	−10.7[b,c]

[a]Gas phase. [b]Acetonitrile. [c]PBE0/TZVP level of theory.

mixture was reduced to about 5 mL. The resulting green precipitate was isolated by filtration, washed twice with EtOH, and dried in vacuum. Yield: 110 mg (87%). IR (KBr pellet, cm^{-1}): ν 3440 (s), 3053 (w), 3038 (w), 2997 (w), 2964 (s), 2866 (m), 1596 (s, $\nu_{as}(RCO_2^-)$), 1553 (m), 1461 (m), 1405 (s, $\nu_{symm}(RCO_2^-)$), 1363 (m), 1348 (w), 1306 (w), 1293 (w), 1267 (m), 1231 (m), 1200 (w), 1179 (w), 1151 (w), 1110 (w), 1078 (s), 1044 (w), 1014 (w), 979 (w), 928 (w), 908 (m), 882 (w), 846 (m), 824 (s), 820 (m), 765 (m), 735 (s), 705 (s), 669 (m), 627 (m), 613 (w), 608 (w), 542 (w), 490 (w), 468 (w), 428 (w), 416 (w). UV/vis [CH_2Cl_2; λ_{max}, nm (ε, M^{-1} cm^{-1})]: 264 (88000), 305 (18190), 329sh (22360), 368sh (3980), 450sh (362), 650 (78, $^3A_{2g} \rightarrow {}^3T_{1g}$), 912sh (40, $^3A_{2g} \rightarrow {}^1E_g(D)$), 1123 (134, $^3A_{2g} \rightarrow {}^3T_{2g}$). ESI-MS ($CH_3CN$): m/z 937.2 ($\{Ni_2L(\mu\text{-}O_2CC_6H_4S)_2\}^{2+}$). Elem anal. Calcd for $C_{138}H_{176}B_2N_{12}Ni_4O_4S_6 \cdot 3H_2O$ (2515.74 + 54.05): C, 64.50; H, 7.14; N, 6.54. Found: C, 64.38; H, 7.09; N, 6.32. This material was additionally characterized by X-ray crystallography.

*$[Ni_2L(O_2CC_6H_4S)AuPPh_3]ClO_4$ (**4**ClO_4).* To a nitrogen-purged solution of AuCl (25.0 mg, 0.108 mmol) in dichloromethane (50 mL) was added triphenylphosphane (28.8 mg, 0.11 mmol), followed by perchlorate salt **2**ClO_4 (100 mg, 0.096 mmol). The suspension was stirred for 20 min, and then sodium methanolate (5.9 mg, 0.11 mmol) was added. The resulting green solution was stirred for an additional 24 h at ambient temperature and filtered, and the filtrate was combined with a solution of $LiClO_4 \cdot 3H_2O$ (87 mg, 0.54 mmol) in EtOH. After stirring for a further 30 min, the volume of the solution was reduced in vacuo to about 10 mL. The resulting green precipitate was filtered off, washed with EtOH, and dried in vacuo to give 132 mg (91%) of **3** as a green powder. IR (KBr pellet, cm^{-1}): ν 3474 (m), 3073 (w), 3050 (w), 2960 (s), 2864 (m), 2807 (w), 2741 (w), 1587 (s, $\nu_{as}(RCO_2^-)$), 1541 (m), 1507 (w), 1481 (w), 1461 (s), 1437 (w), 1422 (w), 1403 (s, $\nu_{symm}(RCO_2^-)$), 1363 (w), 1309 (w), 1291 (w), 1263 (m), 1233 (m), 1201 (w), 1171 (w), 1153 (w), 1098 (s), 1040 (w), 1014 (w), 999 (w), 982 (w), 930 (w), 913 (m), 881 (w), 843 (w), 825 (m), 807 (w), 768 (w), 751 (m), 710 (w), 693 (m), 623 (m), 600 (w), 564 (w), 538 (m), 509 (w), 418 (w). UV/vis [CH_2Cl_2; λ_{max}, nm (ε, M^{-1} cm^{-1})]: 270 (18857), 308 (19273), 375sh (1469), 456sh (101), 653 (19, $^3A_{2g} \rightarrow {}^3T_{1g}$), 916 (7), 1129 (42, $^3A_{2g} \rightarrow {}^3T_{2g}$). ESI-MS ($CH_3CN$): m/z 1397.4 (60%); calcd for $[Ni_2L(\mu\text{-}O_2CC_6H_4S)\text{-}AuPPh_3]^+$ m/z 1397.4. Elem anal. Calcd for $C_{63}H_{83}AuClN_2Ni_2O_6PS_3 \cdot H_2O$ (1497.34 + 18.02): C, 49.90; H, 5.72; N, 5.54. Found: C, 49.89; H, 5.60; N, 5.28.

*$[Ni_2L(O_2CC_6H_4SH)Au(PPh_3)]BPh_4$ (**4**BPh_4).* The perchlorate salt **4**ClO_4 (150 mg, 0.10 mmol) was dissolved in dichloromethane (40 mL). A solution of $NaBPh_4$ (165 mg, 0.48 mmol) in EtOH (30 mL) was added. The volume of the reaction mixture was reduced to about 5 mL. The green product was isolated, washed twice with EtOH and ether, and dried in vacuo. Yield: 143 mg (83%). IR (KBr pellet, cm^{-1}): ν 3444 (w), 3054 (w), 3032 (w), 2997 (w), 2962 (s), 2863 (w), 2806 (w), 1585 (s), 1541 (m), 1480 (w), 1460 (m), 1437 (w), 1422 (w), 1403 (s), 1363 (w), 1349 (w), 1308 (w), 1290 (w), 1262 (m), 1233 (w), 1201 (w), 1170 (w), 1152 (w), 1101 (w), 1077 (s), 1057 (w), 1040 (w), 1014 (w), 999 (w), 982 (w), 930 (w), 912 (w), 881 (w), 843 (w), 824 (s), 817 (w), 807 (w), 768 (m), 748 (w), 732 (m), 704 (s), 693 (w), 630 (w), 612 (m), 563 (w), 538 (s), 509 (w), 472 (w), 416 (w). UV/vis [CH_2Cl_2; λ_{max}, nm (ε, M^{-1} cm^{-1})]: 269 (16688), 308 (16941), 375sh (1148), 456sh (71), 653 (16, $^3A_{2g} \rightarrow {}^3T_{1g}$), 916 (7), 1130 (37, $^3A_{2g} \rightarrow {}^3T_{2g}$). ESI-MS ($CH_3CN$): m/z 1397.4 (60%); calcd for $[Ni_2L(\mu\text{-}O_2CC_6H_4S)AuPPh_3]^+$ m/z 1397.4. Elem anal. Calcd for $C_{87}H_{103}AuBN_6Ni_2O_2PS_3$ (1717.12 + 18.02): C, 60.19; H, 6.15; N, 4.84. Found: C, 60.27; H, 5.92; N, 4.91.

X-ray Crystallography. Crystals of **3**$(BPh_4)_2 \cdot n$EtOH$\cdot n$$Me_2CO$ were grown by slow evaporation of an EtOH/acetone solution of **3**$(BPh_4)_2$. Single crystals of **4**$BPh_4 \cdot$2EtOH$\cdot$2MeCN were obtained by the slow concentration of an acetonitrile/EtOH (1:1) solution of **4**BPh_4 at ambient conditions. Specimens of suitable quality and size were mounted on the ends of quartz fibers and used for intensity data collection on a STOE IPDS-2T diffractometer, employing graphite-monochromated Mo Kα radiation (0.71073 Å). The intensity data were collected and processed with the program *STOE X-AREA*.[59] Structures were solved by direct methods[60] and refined by full-matrix least squares on the basis of all data against F^2 using *SHELXL-97*.[61] *PLATON* was used to search for higher symmetry.[62] Drawings were produced with *ORTEP-3*.[63] Hydrogen atoms were placed at calculated positions and refined as riding atoms with isotropic displacement parameters. All non-hydrogen atoms were refined anisotropically.

CCDC 915790 [**3**$(BPh_4)_2 \cdot n$EtOH$\cdot n$$Me_2CO$] and CCDC 915791 (**4**$BPh_4 \cdot$2MeCN$\cdot$2EtOH) contain the supplementary crystallographic data for this paper. These data can be obtained free of charge at www.ccdc.cam.ac.uk/conts/retrieving.html [or from the Cambridge Crystallographic Data Centre, 12 Union Road, Cambridge CB2 1EZ, U.K.; fax (international) +44-1223-336-033; e-mail deposit@ccdc.cam.ac.uk].

*Crystal Data for **3**$(BPh_4)_2 \cdot n$EtOH$\cdot n$$Me_2CO$:* $C_{138}H_{176}B_2N_{12}Ni_4O_4S_6$, M = 2515.73, triclinic space group $P\bar{1}$, a = 14.2554(11) Å, b = 23.756(2) Å, c = 24.402(2) Å, α = 87.781(7)°, β = 85.210(7)°, γ = 89.109(7) °, V = 8228.2(12) Å^3, Z = 2, D_c = 1.015 g cm^{-3}, μ = 0.572 mm^{-1}, 59986 reflections collected, 27303 unique (R_{int} = 0.0441). Final GOF = 0.976, R1 [$F^2 > 2\sigma(F^2)$] 0.0869, wR2 (all data) 0.2763, R1 index based on 11090 reflections with $I > 2\sigma(I)$ (refinement on F^2). The exact number of the solvate molecules could not be determined, and electron density attributed to heavily disordered acetonitrile and EtOH molecules was removed from the structure (and the corresponding F_o) with the *SQUEEZE* procedure implemented in the *PLATON* program suite. The coligand and two *tert*-butyl groups were found to be disordered over two positions. Although this disorder was successfully modeled using the SADI instructions implemented in *SHELXL*, the quality of the data set is too low, and the structure can only be used to confirm the atom connectivity.

*Crystal Data for **4**$BPh_4 \cdot$2MeCN$\cdot$2EtOH:* $C_{95}H_{121}AuBN_8Ni_2O_4PS_3$, M = 1891.34, triclinic space group $P\bar{1}$, a = 15.196(5) Å, b = 17.687(5) Å, c = 19.126(5) Å, α = 89.255(5)°, β = 69.672(5)°, γ = 73.124(5)°, V = 4591(2) Å^3, Z = 2, D_c = 1.368 g/cm^{-3}, μ = 2.139 mm^{-1}, 24647 reflections collected, 16089 unique. Final GOF = 0.926, R1 [$F^2 > 2\sigma(F^2)$] 0.0382, wR2 (all data) 0.1056, R1 index based on 13326 reflections with $I > 2\sigma(I)$ (refinement on F^2). One *tert*-butyl group was found to be disordered over two positions at half-occupancy. The DFIX command was used to constrain the bond distances of the acetonitrile and EtOH molecules to 1.14 Å for the C−N triple bond, 1.43 Å for the C−O bond, and 1.50 Å for the C−C bonds.

Contact Angles. The surface hydrophobicity was examined by performing water-contact-angle measurements with a DSA II (Krüss, Hamburg, Germany) contact-angle analyzer. The contact-angle measurements were collected using a 4 μL drop size of deionized, distilled water. At least 10 contact angles per five different locations were averaged.

Theoretical Calculations. The total energies (E) for $[Ni_2L\text{-}(SPh)]^+$, $[Ni_2L(O_2CPh)]^+$, $PhCO_2^-$, and PhS^- (Table 4) and the

dx.doi.org/10.1021/ic500683f | Inorg. Chem. 2014, 53, 10825−10834

reaction energy (ΔE) for the reaction $[Ni_2L(SPh)]^+ + O_2CPh^- \rightarrow [Ni_2L(O_2CPh)]^+ + PhS^-$ were calculated within the DFT approximation using the hybrid PBE0 functional.[64] The triple-ζ valence basis set TZV(P) was used.[65] Relativistic effects were taken into account.[66] Calculations were carried out with the *ORCA* program package.[67,68] In the cases of $[Ni_2L(SPh)]^+$ and $[Ni_2L(O_2CPh)]^+$, the X-ray crystallographic data were used as input geometry for calculation of the total energies. The geometries of O_2CPh^- and PhS^- were fully optimized. The COSMO model was used to account for solvent effects.[69] The dielectric constant was set to 36.6 and the refractive index to 1.344.

XPS Spectra. XPS spectra were obtained on a commercial PHI 5600 spectrometer equipped with two light sources. A monochromatized Al Kα source provided photons with an energy of 1486.6 eV, which was used for the core-level studies. The total energy resolution was 350 meV. The gold foils (Au, purity 99.59%) were cleaned in an ultrasonic bath. The substrate was immersed in a 1×10^{-3} M solution of $\mathbf{2}ClO_4$ in dichloromethane for at least 12 h, washed with dichloromethane and then EtOH, and immediately transferred into the spectrometer. Energy referencing was based on the Au($4f_{7/2}$) peak at 84.0 eV. All samples were studied at room temperature at a pressure of approximately 2×10^{-10} mbar. Spectra were analyzed using CasaXPS.

■ ASSOCIATED CONTENT

Supporting Information

X-ray crystallographic data of $\mathbf{3}(BPh_4)_2 \cdot n$EtOH$\cdot nMe_2$CO and $\mathbf{4}BPh_4 \cdot 2$MeCN$\cdot 2$EtOH in CIF format and experimental and calculated susceptibility and magnetization data for $\mathbf{2}ClO_4$ and $\mathbf{4}BPh_4$. This material is available free of charge via the Internet at http://pubs.acs.org.

■ AUTHOR INFORMATION

Corresponding Author

*E-mail: b.kersting@uni-leipzig.de. Fax: (+)+49 341 973 6199.

Notes

The authors declare no competing financial interest.

■ ACKNOWLEDGMENTS

This work was supported by the Deutsche Forschungsgemeinschaft Grant DFG-FOR 1154 ("Towards molecular spintronics") and the University of Leipzig. J.L. thanks the Sächsische Aufbaubank for an Europäischer Sozialfonds grant.

■ REFERENCES

(1) (a) Mitra, S.; Biswas, H.; Bandyopadhyay, P. *Polyhedron* **1997**, *16*, 447−451. (b) Li-Kao, J.; González, O.; Mariezcurrena, R.; Baggio, R.; Garland, M. T.; Carrillo, D. *Acta Crystalloyr., Sect. C* **1995**, *51*, 2486−2489. (c) Li-Kao, J.; González, O.; Baggio, R. F.; Garland, M. T.; Carillo, D. *Acta Crystalloyr., Sect. C* **1995**, *51*, 575−578. (d) Bashkin, J. S.; Huffman, J. C.; Christou, G. *J. Am. Chem. Soc.* **1986**, *108*, 5038−5039. (e) Bodini, M. E.; Del Valle, M. A. *Polyhedron* **1990**, *9*, 1181−1186. (f) Hegetschweiler, K.; Keller, T.; Baumle, M.; Rihs, G.; Schneider, W. *Inorg. Chem.* **1991**, *30*, 4342−4347. (g) Ainscough, E. W.; Brodie, A. M.; Coll, R. K.; Mair, A. J. A.; Waters, J. M. *J. Organomet. Chem.* **1996**, *509*, 259−264. (h) Kumar, L.; Puthraya, K. H.; Srivastava, T. S. *Inorg. Chim. Acta* **1984**, *86*, 173−178. (i) Al-Saadi, B. M.; Sandstroem, M. *Acta Chem. Scand.* **1982**, *A36*, 509−512.

(2) (a) Dinger, M. B.; Henderson, W. *J. Organomet. Chem.* **1998**, *560*, 233−243. (b) McCaffrey, L. J.; Henderson, W.; Nicholson, B. K.; Mackay, J. E.; Dinger, M. B. *J. Chem. Soc., Dalton Trans.* **1997**, 2577−2586. (c) Henderson, W.; Nicholson, B. K. *Inorg. Chim. Acta* **2004**, *357*, 2231−2236. (d) McCaffrey, L. J.; Henderson, W.; Nicholson, B. K. *Polyhedron* **1998**, *17*, 221−229. (e) Depree, C. V.; Main, L.; Nicholson, B. K.; Roberts, K. *J. Organomet. Chem.* **1996**, *517*, 201−207.

(3) Nomiya, K.; Yokoyama, H.; Nagano, H.; Oda, M.; Sakuma, S. *J. Inorg. Biochem.* **1995**, *60*, 289−297.

(4) Vollano, J. F.; Day, R. O.; Rau, D. N.; Chandrasekhar, V.; Holmes, R. R. *Inorg. Chem.* **1984**, *23*, 3153−3160.

(5) Ma, C.; Zhang, Q.; Zhang, R.; Qiu, L. *J. Organomet. Chem.* **2005**, *690*, 3033−3043.

(6) (a) Schneider, W.; Bauer, A.; Schmidbaur, H. *Organometallics* **1996**, *15*, 5445−5446. (b) Sladek, A.; Schneider, W.; Angermaier, K.; Brauer, A.; Schmidbaur, H. *Z. Naturforsch.* **1996**, *51b*, 765−774.

(7) Cookson, P. D.; Tiekink, E. R. T. *J. Coord. Chem.* **1992**, *26*, 313−320.

(8) Geier, D. A.; Sykes, L. K.; Geier, M. R. *J. Toxicol. Environ. Health, Part B* **2007**, *10*, 575−596.

(9) Melnick, J. G.; Yurkerwich, K.; Buccella, D.; Sattler, W.; Parkin, D. *Inorg. Chem.* **2008**, *47*, 6421−6426.

(10) Jacobsen, F. E.; Cohen, S. M. *Inorg. Chem.* **2004**, *43*, 3038−3047.

(11) Karet, G. B.; Castro, S. L.; Folting, K.; Bollinger, J. C.; Heintz, R. A.; Christou, G. *J. Chem. Soc., Dalton Trans.* **1998**, 67−72.

(12) (a) Helmstedt, U.; Lönnecke, P.; Hey-Hawkins, E. *Inorg. Chem.* **2006**, *45*, 10300−10308. (b) Helmstedt, U.; Lönnecke, P.; Reinhold, J.; Hey-Hawkins, E. *Eur. J. Inorg. Chem.* **2006**, 4922−4930.

(13) (a) Wilton-Ely, J. D. E. T.; Schier, A.; Mitzel, N. W.; Schmidbaur, H. *J. Chem. Soc., Dalton Trans.* **2001**, 1058−1062. (b) Wilton-Ely, J. D. E. T.; Ehlich, H.; Schier, A.; Schmidbaur, H. *Helv. Chim. Acta* **2001**, *84*, 3216−3232.

(14) Helmstedt, U.; Lebedkin, S.; Höcher, T.; Blaurock, S.; Hey-Hawkins, E. *Inorg. Chem.* **2008**, *47*, 5815−5820.

(15) (a) Jadzinsky, P. D.; Calero, G.; Ackerson, C. J.; Bushnell, D. A.; Kornberg, R. D. *Science* **2007**, *318*, 430−433. (b) Heinecke, C. L.; Ni, T. W.; Malola, S.; Mäkinen, V.; Wong, O. A.; Häkkinen, H.; Ackerson, C. J. *J. Am. Chem. Soc.* **2012**, *134*, 13316−13322.

(16) Lehmann, U.; Klingele, J.; Lozan, V.; Steinfeld, G.; Klingele, M. H.; Käss, S.; Rodenstein, A.; Kersting, B. *Inorg. Chem.* **2010**, *49*, 11018−11029.

(17) Kersting, B.; Lehmann, U. Chemistry of metalated container molecules. In *Advances in Inorganic Chemistry*; Eldik, R. v., Hubbard, C. D., Eds.; Elsevier: Berlin, 2009; Vol. *61*, pp 407−470.

(18) Frischmann, P.; MacLachlan, M. J. *Chem. Soc. Rev.* **2013**, *42*, 871−890.

(19) Lozan, V.; Kersting, B. *Inorg. Chem.* **2008**, *47*, 5386−5393.

(20) Hausmann, J.; Klingele, M. H.; Lozan, V.; Steinfeld, G.; Siebert, D.; Journaux, D.; Girerd, J. J.; Kersting, B. *Chem.—Eur. J.* **2004**, *10*, 1716−1728.

(21) Jeremies, A. Master Thesis, Universität Leipzig, Leipzig, Germany, 2012.

(22) Gilbert, T. W.; Newman, L. *Inorg. Chem.* **1970**, *9*, 1705−1710.

(23) Hausmann, J.; Klingele, M. H.; Baars, O.; Lozan, V.; Buchholz, A.; Leibeling, A.; Plass, W.; Meyer, W.; Kersting, B. *Eur. J. Inorg. Chem.* **2007**, 5277−5285.

(24) For some effective sulfur-based metalloligands, see: (a) Hsieh, C.-H.; Chupik, R. B.; Brothers, S. M.; Hall, M. B.; Darensbourg, M. Y. *Dalton Trans.* **2011**, *40*, 6047−6053. (b) Elky Almaraz, E.; Foley, W. S.; Denny, J. A.; Reibenspies, J. H.; Golden, M. L.; Darensbourg, M. Y. *Inorg. Chem.* **2009**, *48*, 5288−5295.

(25) Schmidbaur, H.; Cronje, S.; Djordjevic, D.; Schuster, O. *Chem. Phys.* **2005**, *311*, 151−161.

(26) Schröter, I.; Strähle, J. *Chem. Ber.* **1991**, *124*, 2161−2164.

(27) Fackler, J. P.; Staples, R. J.; Elduque, A.; Grant, T. *Acta Crystallogr.* **1994**, *C50*, 520−523.

(28) Krüger, H.-J.; Holm, R. H. *Inorg. Chem.* **1989**, *28*, 1148−1155.

(29) Franolic, J. D.; Wang, W. Y.; Millar, M. *J. Am. Chem. Soc.* **1992**, *114*, 6587−6588.

(30) Krüger, T.; Krebs, B.; Henkel, G. *Angew. Chem.* **1992**, *104*, 71−72; *Angew. Chem., Int. Ed. Engl.* **1992**, *31*, 54−56.

(31) Beissel, T.; Glaser, T.; Kesting, F.; Wieghardt, K.; Nuber, B. *Inorg. Chem.* **1996**, *35*, 3936−3947.

(32) Kersting, B.; Siebert, D. *Inorg. Chem.* **1998**, *37*, 3820−3828.

(33) Journaux, Y.; Glaser, T.; Steinfeld, G.; Lozan, V.; Kersting, B. *Dalton Trans.* **2006**, 1738−1748.
(34) The $[Ni^{III}Ni^{II}L(mba)Au(PPh_3)]^{2+}$ dication $\mathbf{4}^{2+}$ can also be prepared by chemical oxidation. The addition of 1 equiv of $Cu(ClO_4)_2$ to solutions of $\mathbf{4}ClO_4$ results in the immediate formation of a dark-red solution of the dication $\mathbf{4}^{2+}$. The UV/vis spectrum of the latter solution reveals several strong absorption bands [λ_{max} = 380 nm (ε_{max} = 2910 M^{-1} cm^{-1}), 515 nm (1358 M^{-1} cm^{-1}), 782 nm (2296 $M^{-1}cm^{-1}$)], which are assigned as ligand-to-metal ($RS^{-}\rightarrow Ni^{III}$) charge-transfer transitions. The UV/vis spectrum of the electrochemically generated dication $\mathbf{4}^{2+}$ is identical, showing that the chemical and electrochemical oxidations produce the same species.
(35) Bard, A. J., Ed. *Encyclopedia of Electrochemistry of the Elements*; Marcel Dekker: New York, 1975; Vol. *4*, pp 101 ff.
(36) Uson, R.; Laguna, A. *Organomet. Synth.* **1986**, *3*, 322−342.
(37) Preliminary electron paramagnetic resonance spectroscopic studies and temperature-dependent magnetic susceptibility measurements of the mixed-valent $Ni^{III}Ni^{II}$ complex $\mathbf{4}(ClO_4)_2$ reveal an $S = {}^3/_2$ spin system that is attained by a ferromagnetic exchange interaction (J = +8 cm^{-1}; $H = -2JS_1S_2$) between a Ni^{II} ($S_1 = 1$) and a low-spin Ni^{III} ($S_2 = {}^1/_2$) ion. The results of these investigations will be published elsewhere.
(38) Jocelyn, P. C. *Eur. J. Biochem.* **1967**, *2*, 327−331.
(39) Kahn, O. *Molecular Magnetism*; VCH-Wiley: New York, 1993.
(40) Azuah, R. T.; Kneller, L. R.; Qiu, Y.; Tregenna-Piggott, P. L. W.; Brown, C. M.; Copley, J. R. D.; Dimeo, R. M. J. *J. Res. Natl. Inst. Stand. Technol.* **2009**, *114*, 341−358.
(41) Lach, J.; Hahn, T.; Kersting, B.; Kortus, J. *Eur. J. Inorg. Chem.* **2012**, 2381−2388.
(42) Heroux, K. J.; Quddusi, H. M.; Liu, J.; O'Brien, J. R.; Nakano, M.; del Barco, E.; Hill, S.; Hendrickson, D. N. *Inorg. Chem.* **2011**, *50*, 7367−7369.
(43) Sumerlin, B. S.; Lowe, A. B.; Stroud, P. A.; Zhang, P.; Urban, M. W.; McCormick, C. L. *Langmuir* **2003**, *19*, 5559−5562.
(44) Ciszek, J. W.; Stewart, M. P.; Tour, J. M. *J. Am. Chem. Soc.* **2004**, *126*, 13172−13173.
(45) The different solubilities of α- and β-cyclodextrin are a representative example. See: Steed, J. W.; Atwood, J. L *Supramolecular Chemistry*, 2nd ed.; John Wiley & Sons: Chichester, U.K., 2009; pp 327−336.
(46) (a) Wells, M.; Dermody, D. L.; Yang, H. C.; Kim, T.; Crooks, R. M.; Ricco, A. J. *Langmuir* **1996**, *12*, 1989−1996. (b) Barriet, D.; Yam, C.-M.; Shmakova, O. E.; Jamison, A. C.; Lee, T. R. *Langmuir* **2007**, *23*, 8866−8875.
(47) Bain, C. D.; Troughton, E. P.; Tao, Y.-T.; Evall, J.; Whitesides, G. M.; Nuzzo, R. G. *J. Am. Chem. Soc.* **1989**, *111*, 321−335.
(48) Ratel, M.; Branca, M.; Breault-Turcot, J.; Zhao, S. S.; Chaurand, P.; Schmitzer, A. R.; Masson, J.-F. *Chem. Commun.* **2011**, 10644−10646.
(49) This assignment is further supported by XPS spectra for $[Ni_2L(O_2CC_6H_4PPh_2)]ClO_4$, which has only the bridging thiophenolate sulfur atoms. The S(2p) signals for these sulfur atoms are observed at 164 [$S(2p_{3/2})$] and 165 eV [$S(2p_{1/2})$], as in $\mathbf{2}ClO_4$. The $[Ni_2L(O_2CC_6H_4PPh_2)]ClO_4$ compound is attached via a phosphorus atom to a gold surface. Golecki, M.; Lach, J.; Jeremies, A.; Lungwitz, F.; Fronk, M.; Salvan, G.; Zahn, D. R. T.; Park, J.; Krupskaya, Y.; Kataev, V.; Klingeler, R.; Büchner, B.; Mahns, B.; Knupfer, M.; Siles, P. F.; Schmidt, O. G.; Reis, A.; Thiel, W. R.; Breite, D.; Abel, B.; Kersting, B. *Chem.—Eur. J.* **2013**, *19*, 7787−7801.
(50) Laibnis, P. E.; Whitesides, G. M.; Allara, D. L.; Tao, Y.-T.; Parikh, A. N.; Nuzzo, R. G. *J. Am. Chem. Soc.* **1991**, *113*, 7152−7167.
(51) Wells, M.; Dermody, D. L.; Yang, H. C.; Kim, T.; Crooks, R. M.; Ricco, A. J. *Langmuir* **1996**, *12*, 1989−1996.
(52) Copperthwaite, R. G.; Lloyd, J. *J. Chem. Soc., Dalton Trans.* **1977**, 1117−1121.
(53) Matienzo, L. J.; Yin, L. I.; Grim, S. O.; Swartz, W. E., Jr. *Inorg. Chem.* **1973**, *12*, 2762−2769.
(54) Gao, T.; Norby, P.; Okamoto, H.; Fjellvåg, H. *Inorg. Chem.* **2009**, *48*, 9409−9418.
(55) Preda, I.; Gutiérrez, A.; Abbate, M.; Yubero, F.; Méndez, J.; Alvarez, L.; Soriano, L. *Phys. Rev. B* **2008**, *77*, 075411−1−7.
(56) An analysis of the SAM stoichiometry shows a Ni/S atomic ratio of 0.24 rather than the nominal value (0.66), which is attributed to the low intensity of the nickel and sulfur signals.
(57) Whelan, C. M.; Barnes, C. J.; Walker, C. G. H.; Brown, N. M. D. *Surf. Sci.* **1999**, *425*, 195−211.
(58) Under our experimental conditions, $E(Cp_2Co^+/Cp_2Co)$ = −1.345 V vs $E(Cp_2Fe^+/Cp_2Fe)$; $E(Cp_2Co^+/Cp_2Co)$ = −0.937 V vs SCE. Connelly, N. G.; Geiger, W. E. *Chem. Rev.* **1996**, *96*, 877−910.
(59) *IPDS and X-Red32*; Stoe & Cie: Darmstadt, Germany, 2008
(60) Sheldrick, G. M. *Acta Crystallogr.* **1990**, *A46*, 467−473.
(61) Sheldrick, G. M. *SHELXL-97, Computer program for crystal structure refinement*; University of Göttingen: Göttingen, Germany, 1997.
(62) Spek, A. L. *PLATON; A Multipurpose Crystallographic Tool*; Utrecht University: Utrecht, The Netherlands, 2000.
(63) Farrugia, L. J. *J. Appl. Crystallogr.* **1997**, *30*, 565−568.
(64) Adamo, C.; Barone, V. *J. Chem. Phys.* **1999**, *110*, 6158−6170.
(65) (a) Schaefer, A.; Horn, H.; Ahlrichs, R. *J. Chem. Phys.* **1992**, *97*, 2571−2577. (b) Pantazis, D. A.; Chen, X. Y.; Landis, C. R.; Neese, F. *J. Chem. Theory Comput.* **2008**, *4*, 908.
(66) Van Wüllen, C. *J. Chem. Phys.* **1998**, *109*, 392−399.
(67) (a) Neese, F. *J. Chem. Phys.* **2003**, *119*, 9428−9444. (b) Neese, F. *Int. J. Quantum Chem.* **2001**, *83*, 104−114.
(68) Neese, F. *ORCA*, version 2.8; http://www.thch.uni-bonn.de/tc/orca/.
(69) Klamt, A.; Schüürmann, G. *J. Chem. Soc., Perkin Trans. 2* **1993**, *220*, 799−805.